Proceedings of the 2006 IEEE International Conference on Robotics and Automation
Orlando, Florida - May 2006

The Design of a Friction Compensation Control Architecture for a Heavy Lift Precision Manipulator in Contact with the Environment

Justin R. Garretson, William T. Becker, and Steven Dubowsky
Field and Space Robotics Laboratory
Massachusetts Institute of Technology
Cambridge, MA, USA
{jgarrets|beckerw|dubowsky}@mit.edu

***Abstract* – Joint friction is a major obstacle in heavy-lift precision manipulator performance. Friction compensation is vital to the performance of these manipulators. This paper presents a friction compensation architecture for a six degree-of-freedom heavy lift manipulator which utilizes sensor-based compensation in some joints, and a combination of adaptive, and model-based compensation in the remaining joints. The adaptive approach is used when the manipulator is not in contact with the environment, and the model-based compensation is used when the manipulator or its payload nears the environment. The parameters of the model-based approach are updated by the adaptive compensation during the non-contact phase of the task. This approach is validated in simulation.**

Index Terms –heavy lift manipulator, precision manipulator, friction compensation, position control, adaptive control

I. INTRODUCTION

Joint friction presents a major challenge for heavy lift manipulators. The large motors and high gear-ratio transmissions used in the joints of these manipulators have high friction, which results in tracking errors, stick-slip, and other generally undesired behaviors. In some cases, these problems may be overcome by raising system control gains. However, in many manipulators with heavy payloads, low structural natural frequencies introduce stability concerns that limit the control gains that may be used. This paper presents a friction compensation architecture for a precision manipulator with very large payloads (on the order of tons), where the task requires the payload to come in contact with the environment. This control architecture is designed for a teleoperated six degree-of-freedom manipulator mounted on an omni-directional vehicle base to be used for manipulating and transporting large payloads on the deck of a ship, as seen in Fig. 1. This payload must be inserted into slots with tolerances on the order of millimeters. Simulation of this manipulator shows that its behavior is unacceptable in the presence of uncompensated joint friction. In order to satisfy performance requirements, a dedicated friction compensation architecture has been implemented. This system is designed to ensure that friction does not unacceptably degrade manipulator performance, in spite of contact with the environment and changes in the friction over time. Disturbances due to ship motions have been studied, but are beyond the scope of this paper and are not discussed.

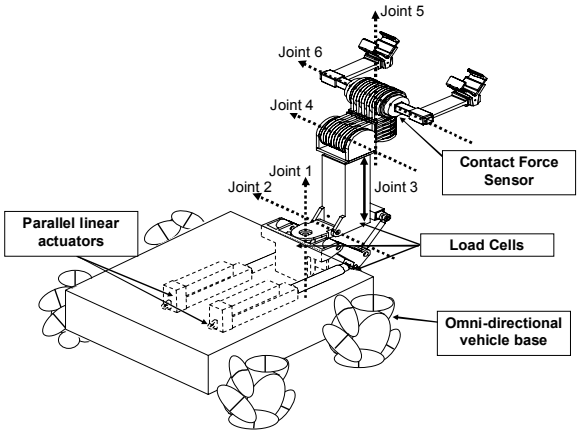

Fig. 1 Manipulator joint definitions (courtesy of Foster Miller Inc.)

Many control methods have been suggested to help systems estimate and compensate for the effects of joint friction [1]. These methods generally fall into three categories: model-based compensation, adaptive compensation, and sensor-based compensation.

Model-based friction compensation uses mathematical models to predict joint friction, which is then compensated with motor torque [2,3]. The effectiveness of this type of compensation depends on the accuracy of the models. Accurate characterization of joint friction is difficult in harsh environments such as this one, as friction will change over time with variations in temperature or wear [4].

To compensate for friction variations, methods have been proposed for online estimation of friction parameters using adaptive and observer-based approaches [1,5,6,7]. These methods take advantage of known or measured information about the system dynamics to identify friction parameters online. Online parameter identification has resulted in good performance in systems with high joint friction [8,9]. The formulation of adaptive methods is very complex, especially for high-degree-of-freedom systems [10]. Adaptive identification is not practical for some systems, because adaptive identification may view contact forces as frictional disturbances, and may become unusable when the manipulator is in contact with the environment.

Sensor-based compensation overcomes many of the problems of model-based and adaptive methods. These methods can be employed when there are sensors available to

provide direct feedback of the system friction. Torque control loops can then be used to reduce the effects of friction [11,12]. No model of the friction is required and the compensation is robust to friction changes with wear or temperature. This method has been shown to provide accurate compensation for joint friction, however, providing sensors at each joint can be costly and add to system complexity. More recently, an alternative sensor-based method has been proposed that allows the friction in all joints to be identified using a single six-degree-of-freedom force/torque sensor in the manipulator's base, greatly simplifying the hardware implementation of sensor-based approaches [13].

Sensor-based methods are preferred when the sensor hardware is available for all joints. Adaptive methods can perform very well, but cannot handle contact forces. Model-based methods are more stable, but are not robust to unmodeled or time-varying effects. The system in this paper has low structural natural frequencies, so gains cannot be raised to overcome friction. Force sensors are not present at some joints, and the manipulator is required to come in contact with the environment. However, a simple model-based compensator is insufficient for the friction variations caused by the harsh environment of the deck of a ship. This paper presents a practical friction compensation architecture that utilizes a combination of sensor-based, model-based, and adaptive approaches for this system. The hardware for this robot is under construction, so experimental validation of the algorithms developed in simulation will be reported in the near future.

Simulations show that the friction can be compensated by on-line algorithms so that the performance closely matches a frictionless case. In addition, a friction model can be accurately identified and used in a feed-forward compensator when the manipulator is in contact with the environment.

II. System Description

A. Joint Configuration

The system to be controlled is shown in Fig. 1. Joints one and two are base yaw and pitch joints, respectively. The two joints are dependently linked to each other, and actuated by parallel linear actuators mounted on the base of the robot. Joint three is a prismatic joint which extends the end three joints from the base. Joint four is an end pitch joint, and joint five is an end yaw joint. Joint six pitches or rolls the payload, depending on joint configuration. The end-effector is a pair of fork tines which can either be inserted into a pallet (like a fork-lift) for larger payloads, or fitted with grippers to grasp smaller payloads. The actuators for the first three joints are linear actuators powered by gear-motors with roller-screw transmissions. The actuators on the end three joints are proprietary high-torque direct-drive motors.

B. Sensors and User Interface

The robot is equipped with high-accuracy encoders to measure joint position. In the first three joints, load cells are located after the transmission, enabling observation of the actual force applied by each linear actuator. Force sensors are not present in the other three joints due to mechanical design constraints. A six-axis force-torque sensor is in place so that contact forces on the payload can be identified. A three-axis translational accelerometer is located in the base of the manipulator in order to compensate for ship motions and inclined floor surfaces. The user interfaces are a joystick on the omni-directional base, and a force-sensing handle located near the payload.

C. Friction Models

Laboratory tests of the motors used in the base joints and the end joints reveal that very different friction profiles exist in each group of joints.

The friction behavior in the base joints resembles a standard friction profile with coulomb and viscous components and some stick-slip behavior, as well as a linear dependence on the static load on the motor. The friction model (1) was extracted from the experimental data, and the model is shown in Fig. 2a for constant static load. α_1 and α_2 define coulomb friction and the effect of static load. α_3 defines the contribution of viscous friction. The β terms define a nonlinear velocity-dependent shaping function to approximate the stick-slip model. Further information on this approximation can be found in [1,4].

$$\tau_{friction} = -[(\alpha_2 + \alpha_1 F_{load})(\beta_1 + \beta_1(1 - e^{-\beta_1|\dot{q}|}) + \alpha_3|\dot{q}|]\mathrm{sgn}(\dot{q}) \qquad (1)$$

Because the end three joints employ direct-drive motors, the only significant source of friction in those joints is from the motors themselves. This friction profile, given by (2), exhibits a linear dependence on joint velocity, and a quadratically decreasing dependence on the motor load. Stick-slip effects were not significant. α_1 defines the velocity-dependent term, α_2 defines the zero-velocity, zero-load level of friction, and α_3 and α_4 define the contribution of motor load to the friction. The friction model with respect to motor load is shown for a constant velocity in Fig. 2b.

$$\tau_{friction} = -(1 + \alpha_1|\dot{q}|)(\alpha_2 + \alpha_3|\tau_{motor}| + \alpha_4 \tau_{motor}^{\ 2})\mathrm{sgn}(\dot{q}) \qquad (2)$$

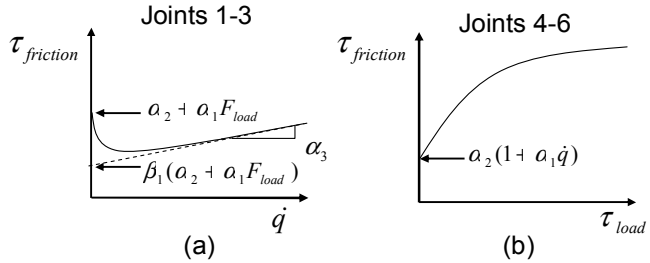

Fig. 2 (a)Friction models for joints 1-3 as a function of velocity at constant load, and (b) joints 4-6 as a function of motor load at constant velocity

D. Performance Goals

The manipulator must handle payloads of up to 1350 kg. Payloads of up to 225 kg have complex insertion constraints with 2 mm tolerances, while larger payloads have a simple, straight peg-in-hole insertion with friendly geometry and

tolerances of 1.0 cm. Throughout this paper, reference to a heavy payload is to a 1350 kg payload with the simple insertion, and reference to a light payload is to a 135 kg payload requiring a complex insertion. The goal is to be able to meet these tolerances during insertion, and to have no greater than a 2.5 cm tracking error at any point while the manipulator is maneuvering the payload.

III. Control Architecture

The controller shown in Fig. 5 has two user-selectable modes. These are a teleoperated position control mode, which is used when maneuvering the payload away from obstacles, and an insertion control mode, which is used when the payload is near or in contact with the environment.

The user has a choice of two methods of inputting the position commands. Direct joint control is used when the user needs the manipulator to move into a specific pose, such as for transporting the payload, or when the manipulator is in a near-singular configuration. For all other times, a user inputs a desired translational and rotational velocity for the payload. This desired Cartesian-space trajectory is translated into desired joint positions by a resolved-rate controller, which multiplies the desired Cartesian velocity by the inverse manipulator Jacobian, and then integrates the output into a desired joint position [14].

The other controller mode gives a more intuitive control when the user needs to insert the payload into its slot. The user inputs a force at a six-axis force handle near the end-effector. Another force-torque sensor under the payload is used to give a measure the contact force on the payload, which is added to the user force input. The contact force acts as feedback so the user cannot force the payload into the environment. The combined force signal is translated into a desired Cartesian velocity by an admittance law, which is then input to the resolved-rate controller as before, and output as desired joint positions.

In both control modes, the actual and desired joint positions are then input to the joint PID controllers. In general, higher gains are desirable in order to properly track the desired trajectory. However, in this manipulator, structural resonances of between 5 Hz (heavy payload) and 9Hz (light payload) limit the bandwidth of the controller. Gains are scheduled on a per-payload basis, and tuned so that the bandwidth of each joint controller is set to a decade below the structural resonance of

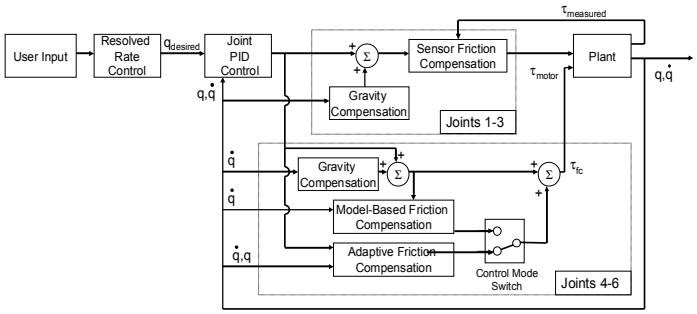

Fig. 5 Block diagram of control architecture

the system. The structural resonances of the system vary between 5 Hz and 9 Hz, so the bandwidths of the joint controllers are set to between 0.5 Hz and 0.9 Hz with a damping ratio of 0.7.

The effects of gravity and ship motions are significant in this system. Gravity and ship motion compensation are needed to ensure the system response is predictable, and the disturbances from uncompensated gravity or motions do not lead to tracking errors. The gravity compensation is calculated using a feed-forward model and uses accelerometers in the base to compensate for base tilt and ship motions. Gravity and friction compensating torques are summed with the output torque from the PID controllers.

IV. Friction Compensation Control Architecture

Three forms of friction compensation are used in the architecture. As previously mentioned, load cells are located after the transmissions for the motors acting on the three joints closest to the base of the manipulator. These allow a sensor-based method called torque loops to be used. There are no joint force sensors on the end three joints, so this is not an option. During position control mode, an adaptive algorithm is used to identify friction parameters for these joints. During insertion control, the payload is required to come into contact with the environment, which makes adaptive compensation difficult. Therefore, in insertion control a model-based feed forward algorithm based on the friction parameters learned by the adaptive controller during the non-contact mode is used in the end three joints. The first three joints continue to use sensor based inner torque loops to compensate for friction.

A. Joints 1-3: Torque Control

The force sensors in the first three joints of the manipulator are located between the end of the roller screw of the linear actuators that power the joints, and the linkage of the joint itself. This allows a reliable measurement of the force transmitted through this point in the manipulator. The force at the end of the linear actuator is related to the motor torque by:

$$F_{Loadcell} = \tau_{measure} \frac{2\pi R_g}{L} \tag{3}$$

where L is the lead of the roller screw, and R_g is the transmission gear ratio. This measured torque is fed back into a torque control loop. The error between this measured torque and the desired torque is input into a PI controller, so that actual torque applied to the joint tracks that desired by the PID position controller and gravity compensation [11]. The gains in the torque control loops have been selected so that their bandwidth is approximately ten times the bandwidth of the PID controllers, which makes the dynamics of the torque loops effectively invisible to the overall system.

B. Joints 4-6: Adaptive Control

The adaptive estimator used in this manipulator was originally proposed by Friedland and Park [15]. This method has been shown to provide accurate online estimates of friction

in position control systems [9,16,17]. Like most adaptive algorithms, the Friedland-Park algorithm is based on a dynamic model of the joint:

$$\tau_{app} + \tau_{fric} = J\alpha \tag{4}$$

where J is the effective joint inertia, α is the joint angular acceleration, τ_{app} is the applied torque by the controller, and τ_{fric} is the disturbance torque, which is assumed to be friction. The effective joint inertia is a function of the manipulator configuration, and is defined as the moment of inertia of the links of a manipulator beyond a joint, about that joint. The applied torque (τ_{app}) is the sum of the uncompensated torques commanded to the joint by the controller. In this manipulator, the applied torque (5) is the sum of contributions of the PID controllers (τ_{PID}) and the friction compensation torque (τ_{fc}). Disturbance torques come from many sources, such as friction, wind, contact forces, or errors in the gravity compensation.

$$\tau_{app} = \tau_{PID} + \tau_{fc} \tag{5}$$

The Friedland-Park algorithm identifies the magnitude of the disturbance force (â) through the use of an observer. It is assumed that all disturbances are the result of friction in the joint, and the algorithm attempts to identify and cancel out this disturbance. The algorithm will converge to the actual value of the disturbance so long as there is sufficient joint excitation for the observer. For practical purposes, this means that the algorithm will work well whenever the joint is moving, except during an initial learning period. A friction compensation torque is then applied as the estimated magnitude â times the sign of the velocity (6) through the control law (7). The intermediate variable z is found using the adaptation law (8):

$$\tau_{fc} = \hat{a}\,\mathrm{sgn}(\dot{q}) \tag{6}$$

$$\hat{a} = z - Jk\left|\dot{q}\right|^{\mu} \tag{7}$$

$$\dot{z} = k\mu\left|\dot{q}\right|^{\mu-1}[\tau_{app} - \tau_{fc}]\,\mathrm{sgn}(\dot{q}) \tag{8}$$

where q is the joint angle and k and μ are gains tuned for individual joints. In the case of this manipulator, the applied torque less the friction compensation torque is the torque from the PID controllers. Fig. 6 is a block diagram of the adaptive friction compensation algorithm, and shows the inputs and outputs as well as the adaptation and control laws.

C. Joints 4-6: Model-Based Feed Forward Algorithm

Adaptive compensation is not feasible for the end three joints when the manipulator comes into contact with the environment. The contact forces are interpreted by the Friedland-Park algorithm as friction, and the algorithm would go unstable as it attempted to compensate for them. Hence, model-based compensation is selected for these joints. Pre-determined models of the friction degrade over time, so estimates of the friction from the adaptive compensation used during the position control mode are used to curve-fit

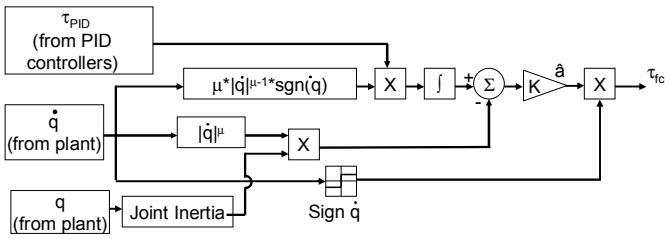

Fig. 6. Block diagram of adaptive compensation algorithm

parameters to a known form of friction model (2). To fit data this model, the adaptive friction estimate, motor torque, and joint velocity are recorded during the position control mode. A curve-fit of recent adaptive data is performed to identify the friction model parameters. Accurate parameter identification of the model requires that the data be filtered to eliminate spurious data points. These filters reduce the sampling rate of the recorded data for computational speed, remove data where joint velocity is near zero velocity, and remove data during initial learning transients. A least-squares curve fit is performed with the data, and the parameters σ_1, σ_2, σ_3, and σ_4 are identified. The friction compensation torque is then calculated by substituting the values of motor torque and joint velocity into equation (2).

V. RESULTS

A dynamic simulation of the full system was used to verify the friction compensation algorithms. A representative model for heavy and light payload cases using specified inertia and kinematic values were constructed in MSC ADAMS, and interfaced with a Simulink controller running at a time step of 0.001 s. The PID gains used in the joint controllers were tuned to be below 0.1 of the lowest structural natural frequency of the system obtained from an independent finite element analysis. The joint friction was implemented in the Simulink controller utilizing the models described in section II.C.

A. Representative Tasks

Fig. 7 and 8 show the performance of the manipulator tracking a desired Cartesian and joint-space trajectory. Separate trajectories for the heavy and the light payloads were chosen to represent actual shipboard tasks. The simulations characterize the position control section of each representative task, and compared the performance of the manipulator with friction compensation to a case with zero friction, and to a case with no friction compensation. Except during the insertion phase in both tasks, a tracking error specification of less than 2.5 cm was used. During insertion, the tracking error for a large payload can be no more than 1 cm, and for a small payload can be no more than 2 mm. The tracking error results are seen in Fig. 7 for the heavy payload, and in Fig. 8 for the light payload, and include a case with no friction, a case with uncompensated friction, and a case with compensated friction.

Both figures show that the error in the friction compensated case is almost indistinguishable from the error in

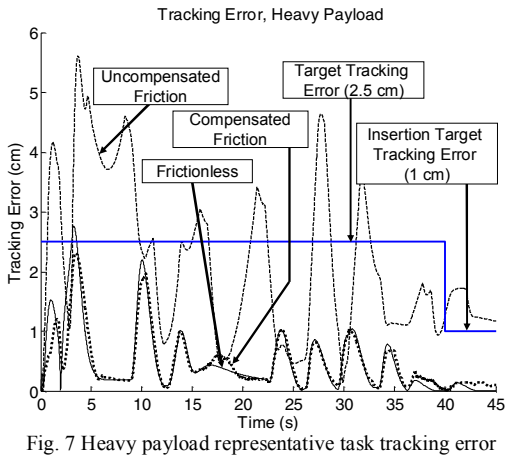

Fig. 7 Heavy payload representative task tracking error

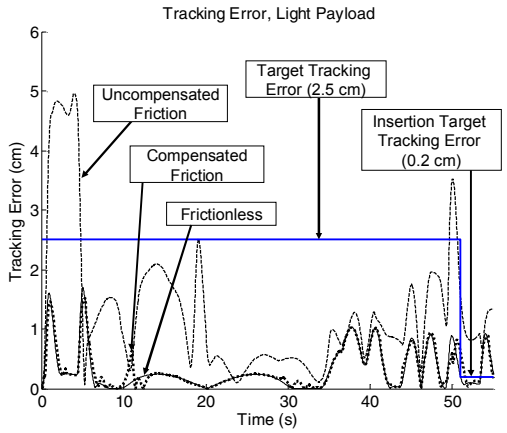

Fig. 8 Light payload representative task tracking error

the frictionless case, and both are large improvements over the uncompensated friction case. It can be seen from Fig. 7 that the accuracy of the position controller is satisfactory over the entire representative task for the heavy payload. Fig. 8 shows that while the performance of the manipulator with the light payload is satisfactory for most of the motion, it is not accurate enough during insertion, and requires the insertion controller for successful completion. Comparing the frictionless cases in Fig. 7 and 8 to the compensated friction cases shows that the errors are due more to the slow bandwidth of the PID controllers rather than uncompensated friction. In practice, the insertion controller will be used during insertion for all payloads because of the presence of contact forces, but it is reassuring to know that the position controller has accuracy of the same order of magnitude as the constraints of the insertion.

B. Repeatability Test

An important measure of performance is repeatability, which is a measure of how well a controller can move to a given position with consistent results. To test this, a simulation was run of the manipulator with a heavy payload under position control to see how well it could move away from and return to a given point in its workspace. It was commanded to move at a set speed to a random distance and direction away from a point, and then return to that point; after two seconds of settling time, the endpoint position was

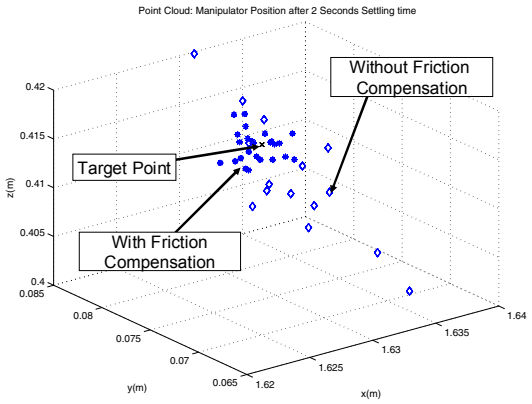

Fig. 9 Results of the repeatability study

measured. This test was performed using sensor-based friction compensation in the first three joints and adaptive compensation in the end three joints. The same test was then performed without friction compensation. A point cloud of the endpoint locations for the two cases is shown in Fig. 9.

C. Friction Model Extraction and Comparison

An algorithm was developed for extracting a friction model as detailed in section IV.C. The data extraction for joint six of the light payload motion is considered in this section. The adaptive estimator performance for joint six of the manipulator is shown in Fig. 12. The adaptive estimate closely matches the actual value of friction whenever the velocity is sufficiently away from zero.

In order to accurately identify the parameters of the

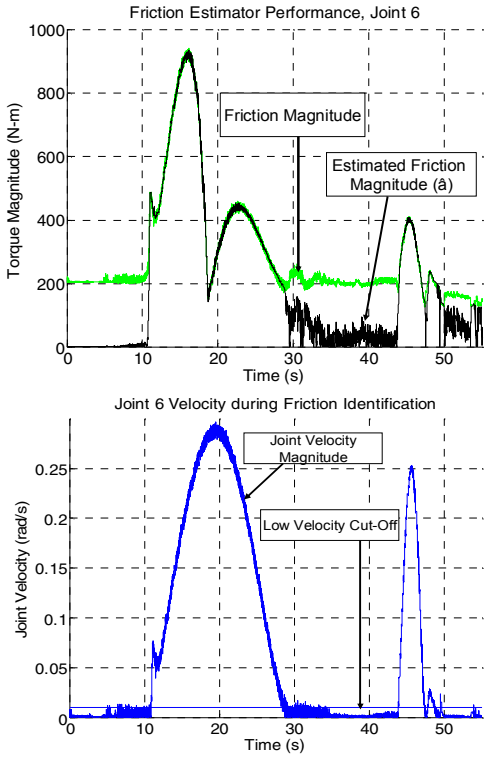

Fig. 10. Adaptive friction estimator performance for joint 6 during the light payload task.

friction model, data points taken when the joint velocity was lower than 0.01 rad/s were excluded. All points on the initial learning curve (all points before the joint velocity reached 0.02 rad/s for the first time) were removed. The non-linear curve-fit accurately identified the parameters of the friction model, as seen in Table 1.

TABLE I
ACTUAL AND IDENTIFIED FRICTION MODEL PARAMETERS

	α_1	α_2	α_3	α_4
Actual Parameters	10	350	0.187	-1e-6
Identified Parameters	10.19	352.29	0.182	-1.3e-6

Fig. 11 shows a comparison between the adaptive estimates of friction, actual values of friction, and the curve-fit modelled value of friction from the light payload trajectory of Joint 6. It can be seen that the errors are effectively zero. The model has a maximum percent error of 1.99%, and an average percent error of 0.40% at the points used for the curve-fit. Note in the simulation the form of the model that the data is the same as that used by the model-based compensator. Future studies are underway to examine the ability of this approach to estimate the friction when the form of the friction is not well known.

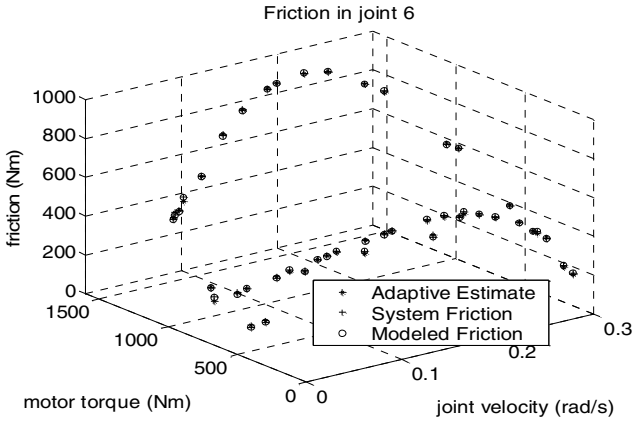

Fig. 11. Comparison of the adaptive friction estimates with the system friction and curve-fit model friction.

VI. CONCLUSIONS

A friction compensation architecture containing three compensation methods of compensation has been designed in order to meet the constraints of the shipboard manipulation task. The results show that the friction compensation architecture demonstrably decreased the tracking error due to joint friction so that the performance of the manipulator with friction compensation was almost indistinguishable from the frictionless case. The adaptive friction compensators accurately identified the magnitude of the friction. This identification of the friction magnitude allows an algorithm to accurately identify parameters of a friction model for the end three joints when the manipulator is in contact with the environment. While the overall accuracy of this model is dependent on how accurate the form of the model imitates reality, the accuracy of the adaptive estimates ensures that if the form of the model is correct, the estimation of the parameters will converge. Simulations suggest that the manipulator will be able to fulfil its goal of inserting a wide variety of payloads. Continuing work on this project includes performance testing of the insertion control algorithm, and hardware testing of the control architecture.

ACKNOWLEDGEMENTS

The authors would like to thank Foster-Miller, Inc. for their support of this research, as well as Matt Dicicco, Takeshi Takaura, and Matt Lichter for their helpful comments and contributions during this work.

REFERENCES

[1] Armstrong B, Dupont P, Canudas C. "A Survey of Models, Analysis Tools and Compensation Methods for the Control of Machines with Friction." Automatica, Vol. 30, Issue 7, pp. 1083-1138, July 1994.
[2] Gomes S, Santos da Rosa V. "A New Approach to Compensate Friction in Robotic Actuators." Proceedings. ICRA '03. IEEE International Conference on Robotics and Automation, Vol. 1, 14-19, September 2003.
[3] Moreno J, Kelly R, Campa R. "Manipulator Velocity Control using Friction Compensation." IEE Proceedings on Control Theory Applications, Vol. 150, No. 2, March 2003.
[4] Olsson H, Astrom K, Canudas C, Gafvert M, Lichinsky P. "Friction Models and Friction Compensation." European Journal of Control, Vol. 4, No. 3, 1998.
[5] Canudas C, Lischinsky P. "Adaptive Friction Compensation with Partially Known Dynamic Friction Model." International Journal of Adaptive Control and Signal Processing, Vol. 11, 65-80, 1997.
[6] Henrichfreise H, Witte C. "Experimental Results with Observer-Based Nonlinear Compensation of Friction in a Positioning System." IEEE Intl. Conference on Robotics and Automation, Vol. 1, 16-20, May 1998.
[7] Friedland B, Mentzelopoulou S. "On Estimation of Dynamic Friction." Proceeding of the 32nd Conference on Decision and Control, Vol. 2, 15-17, pp. 1919-1924, December 1993.
[8] Lischinsky P, Canudas C, Morel G. "Friction Compensation of a Schilling Hydraulic Robot," Proceedings of the 1997 IEEE International Conference on Control Applications, 5-7, pp. 294-299, October 1997.
[9] Kim H, Cho Y, Lee K. "Robust Nonlinear Task Space Control for a 6 DOF Parallel Manipulator." Proceedings of the 41st IEEE Conference on Decision and Control, Vol. 2, 10-13, December 2002.
[10] Niemeyer G, Slotine J. "Performance in Adaptive Manipulator Control." Proceedings of the 27th IEEE Conference on Decision and Control, Vol. 2, 7-9, pp. 1585-1591, December 1988.
[11] Luh J, Fisher W, Paul R. "Joint Torque Control by Direct Feedback for Industrial Robots." IEEE Transactions on Automatic Control, Vol. 28, No. 1, Feb. 1983.
[12] Pfeffer L, Khatib O, Hake J. "Joint Torque Sensory Feedback of a PUMA Manipulator." IEEE Transactions on Robotics and Automation, Vol. 5, No. 4, pp. 418-425, 1989.
[13] Iagnemma K. "Manipulator Identification and Control Using a Base-Mounted Force/Torque Sensor." Master's Thesis, Department of Mechanical Engineering, MIT, 1997.
[14] Whitney, D.E., "Resolved Motion Rate Control of Manipulators and Human Prostheses." IEEE Transactions on Man-Machine Systems, Vol. MMS-10 No. 2 June 1969.
[15] Friedland B, Park Y. "On Adaptive Friction Compensation." IEEE Transactions on Automatic Control, Vol. 37, Issue 10, pp. 1609-1612, October 1992.
[16] El-Roy A, Friedland B. "Precision Single-Axis Motion Control System with Friction Compensation." Proceeding of the American Control Conference, Vol. 5, 21-23, pp. 3299-3302, June 1995.
[17] Amin J, Friedland B, Harnoy A. "Implementation of a Friction Estimation and Compensation Technique." Control Systems Magazine, IEEE, Vol. 17, Issue 4, pp. 71-76, August 1997.